Assessment of RC elements strengthened with NSM FRP rods by experimental tests

Roberto Capozucca[1,*] and *Erica* Magagnini[2]

[1]Professor of Civil Structural Engineering, DICEA, Polytechnic University of Marche, 60100 Ancona, Italy.
[2]Post-Doctoral, PhD Eng., DICEA, Polytechnic University of Marche, 60100 Ancona, Italy.

Abstract. Near surface mounted (NSM) technique of strengthening with FRP rods inserted in grooves on the concrete cover of damaged RC beams has been improved in recent years. The aim of this paper is the examination of the static and dynamic behaviour of undamaged and damaged reinforced concrete (RC) beams with free-free ends. RC beams strengthened with NSM Glass and Carbon fiber reinforced polymer (G-CFRP) rods have been experimentally analysed. The damage of the RC beam model was obtained by the cracking of concrete under bending tests. The detection of damage and monitoring of RC beams with and without strengthening were carried out by vibration tests assuming free-free ends at different degree of damage. Envelope diagrams of Frequency Response Functions (FRFs) obtained by the dynamic experimental tests are shown and the changes of natural frequency values are correlated to the damage degree of beam elements. Experimental results are discussed with particular emphasis on the aspect of the loss of bond.

1 Introduction

The strengthening of damaged reinforced concrete (RC) beams is a relevant topic of civil engineering. In fact, many causes, such as environmental conditions that result in the corrosion of steel reinforcement and static not foreseen high loads, or more simply errors of design may usually damage reinforced concrete elements. The use of fiber-reinforced composites has increased in recent years and the near surface method (NSM) with FRP rods inserted inside grooves on the concrete cover appears useful to in order to solve many problems [1-4]. Examples of NSM using steel rods for strengthening RC structures go back to the early 1950s; the advantages of FRP rods compared to steel is that they are easier and quicker to assemble due to the lightness of the strengthening materials, the slimness of the grooves attributable to the higher traction resistance and, FRPs' improved corrosion resistance. Furthermore, the NSM strengthening appears capable of solving the susceptibility of FRP sheets or externally bonded FRP reinforcements to damage deriving from collision, high temperature and fire.

* Corresponding author: r.capozucca@staff.univpm.it

The availability of strengthening with NSM FRP strips or rods depends on maintaining the bond between NSM rods and concrete. Many factors affect the bond performance: bonded length, diameter of the FRP rod, type of FRP material, surface configuration of the rod, size of the groove [5-7].

Bond behaviour has an influence on the ultimate capacity of reinforced elements as well as on serviceability aspects such as crack width and spacing. NSM FRP rods are prone to show greater slips than steel reinforcement due to potentially lower bond shear stress of FRP materials [8,9], to the presence of surrounding adhesive layers and local cracking in the cover concrete [9,10].

Investigations and theoretical studies addressing the bond behaviour of FRP rods in RC elements [9,11,12] and describing most of the fundamental aspects of the NSM technique have been developed: an experimental program involving pull-out and bending tests was carried out to evaluate local bond stress-slip relationship by controlling numerically developed strategies [13-14].

Although these methods are destructive in character, direct pull-out tests and bending tests may be adequate for describing bond mechanism and failure modes in NSM strengthening. In addition, an analysis of dynamic responses may be adopted as a non-destructive testing method (NDTM) for investigating the behaviour of RC beams strengthened with NSM FRP rods [12,15]. The basic concept behind vibration monitoring is that dynamic characteristics are functions of structures' physical properties. Therefore any change caused by damage results in a change in dynamic response [15,16]. In the strengthening method, actual bond-slip may be influenced by the cracking of concrete and loss of adhesion of rods which can modify frequency values and beams' modes of vibration.

The aim of this paper is to analyze the static and dynamic behaviour of RC beams damaged and strengthened by both carbon and glass fiber reinforced polymer (C-GFRP) rods utilizing near surface method.

A large investigation concerning both specimens subjected to pull-out tests with NSM FRP rods and bending tests of RC beams with strengthening [13,14] allows to analyze the response of RC elements and define the reliability of the theoretical model. Furthermore, the nondestructive method based on vibration tests adopted during the experiments enables the control of the RC beams at different damage steps due to the cracking of concrete; experimental static and vibration results are discussed and comments on the strengthening of the bond of NSM C-GFRP rods were developed.

2 Analysis of bond and results of pull-out tests

Bond in NSM strengthening has influence on the ultimate capacity of the strengthened RC beams as well as on serviceability aspects of cracking on the surface of concrete, width and spacing. The mechanics of bond are linked to bond stress and slip at the failed interfaces of material. The relative displacement between FRP rod and concrete is the sum of rod-to-epoxy and epoxy-to-concrete slips. If failure occurs at the epoxy-concrete interface, the average bond strength is that at the failed interface [9,14]:

$$\tau_{av,1} = \frac{P_{\max}}{3d_g \cdot l_b} \tag{1a}$$

where: P_{max} is the peak load; d_g is the perimeter of groove size and l_b the bonded length. When a failure mechanism emerges at the interface between rod and groove-filled material, the average bond strength may be computed as:

$$\tau_{av,2} = \frac{P_{\max}}{\pi \cdot d_b \cdot l_b} \tag{1b}$$

where: d_b is the diameter of the FRP rod.

In general, the most dangerous failure mechanism is the loss of bond around the rod at the rod-epoxy interface. An analytical model was developed [14] through an energy approach which allows to obtain bond stress-slip laws and to evaluate the fracture energy value G_f. It assumes failure occurs at the interface between the rod and groove-filling material (Fig. 1): the w(z) function represents the displacement of the point of rod along its axis under applied load. The total energy of the system may be written as the sum of internal energy of deformation and external energy due to load P:

$$\mathrm{E} = \frac{1}{2}\int_0^{l_b} [E_{FRP} \cdot A_{FRP}[w'(z)]^2 + K_{EP} \cdot w^2(z)] \cdot dz - P \cdot w_{z=l_b} \tag{2}$$

where: P is the tensile load; EFRP is the Young's modulus of FRP; AFRP is the cross section of FRP rod; $K_{EP} = \frac{3}{2}\pi \cdot \frac{d_g}{(d_g - d_b)} \cdot G_{EP}$ is the stiffness of resin surrounding the FRP rod (Fig. 1(c)); $\gamma(z) = \frac{w(z)}{t}$ and $\tau(z) = G_{EP} \cdot \gamma(z)$, respectively, the shear strain and stress; G_{EP} the shear modulus of resin. Minimizing the total energy with respect to the w(z) function, the following 2nd order differential equation is obtained:

$$w''(z) - \xi^2 \cdot w(z) = 0 \tag{3}$$

with the coefficient: $\xi = \sqrt{\frac{4 \cdot K_{EP}}{E_{FRP} \cdot \pi \cdot d_b^2}}$.

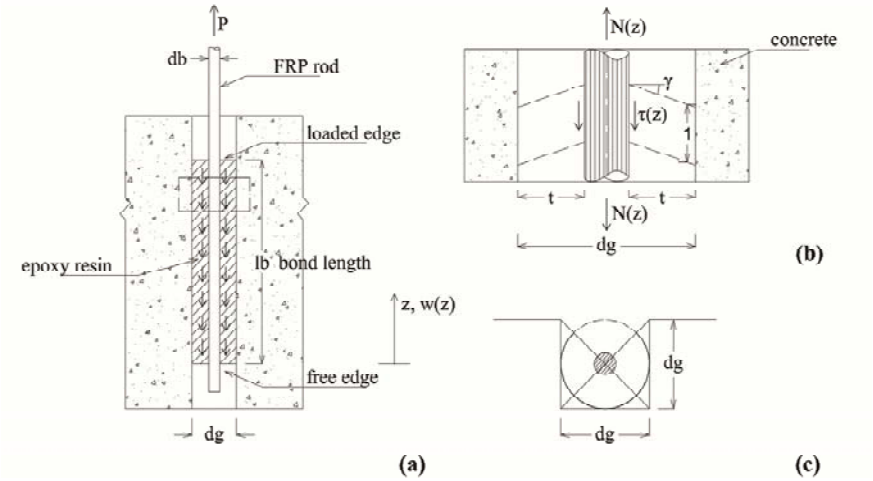

Fig. 1. Analytical model to study the bond mechanisms : (a)vertical section of groove ; (b) detail and cross section of groove with circular FRP rod.

The solution of Eq. (3) is the following function:

$$w(z) = C_1 \cdot \cosh(\xi \cdot z) + C_2 \cdot \sinh(\xi \cdot z) \tag{4}$$

With the following boundary conditions: $\varepsilon(z)\big|_{z=0} = 0$; $\varepsilon(z)\big|_{z=l_b} = \frac{P}{E_{FRP} \cdot A_{FRP}}$ the final expression of displacement function is obtained:

$$w(z) = \frac{P}{\xi \cdot E_{FRP} \cdot A_{FRP}} \cdot \frac{\cosh(\xi \cdot z)}{\sinh(\xi \cdot l_b)} \tag{5}$$

By the Eq. (5), the strain distribution along the rod may be evaluated:

$$\varepsilon(z) = \frac{\sigma_{FRP;z=l_b}}{E_{FRP}} \cdot \frac{\sinh(\xi \cdot z)}{\sinh(\xi \cdot l_b)} \tag{6}$$

Assuming a simplified theoretical bi-linear model of the bond with a softening branch after the maximum shear stress value, the fracture energy G_f is given by:

$$G_f = \frac{1}{2} \cdot \frac{A_b}{E_b \cdot \Sigma_b} \cdot (\sigma_{\max})^2 \cdot \left[\frac{\cosh(\xi \cdot l_b)}{\sinh(\xi \cdot l_b)} \right]^2 \tag{7}$$

where: Σ_b ideal perimeter of the groove. For a sufficiently long bond length, having $\tanh(\xi \cdot l_b) \cong 1$, from the maximum normal stress for the NSM FRP rod is obtained:

$$\sigma_{\max} = \sqrt{2E_b \frac{\Sigma_b}{A_b} G_f} \tag{8}$$

We may note that if tension $\sigma_{\max}$ is lower than the resistance of the FRP bar, the total capacity of the strengthening cannot be developed independently from the length of the rod anchorage; when $\sigma_{\max}$ exceeds the tensile strength of the rod, the total capacity of the strengthening can be developed with infinite values of energy fracture [8] as $G_f = \int \tau(w) dw$.

2.1 Pull-out tests

Experimental investigation foresaw direct pull-out tests on RC elements with one FRP rod inserted into the groove. Dimensions of RC specimens were: length 400mm·150mm·150mm. An epoxy resin characterized by tensile strength $f_{EPOX} \geq 8 N/mm^2$ and Young's modulus equal to $E_{EPOX} = 9.5 \cdot 10^3$ kN/mm^2 was adopted. Specimens were built with different geometry of the section of the FRP and different characteristics evaluated experimentally in laboratory as well; main properties of CFRP rods: tensile strength $f_{CFRP} = 1704.82 N/mm^2$; Young's modulus $E_{CFRP} = 1.24 \cdot 10^5$ N/mm^2; and diameter $d_b = 8mm$; main parameters of the GFRP rod: $d_b = 9.53mm$ $f_{GFRP} = 1040$ N/mm^2 $E_{GFRP} = 33.6 \cdot 10^3 N/mm^2$. Pull-out tests were carried out with different bond length of FRP rods: $l_b = 200mm$ - 250mm and 300mm and the position of strain gauges with an interval of 50mm to measure strain under pull-out tests– are shown. LVDT was used to measure the displacement at the free end of the rod during loading. In Figure 2, a general view of the location of strain gauges and the setup of direct pull-out test is shown.

In Figures 3(a), (b) and (c) the experimental diagrams load versus strain for four strain gauges no. 1, …, 4 on CFRP rods are shown. It may be noted that for a bond length $l_b \leq$ 250mm the strain value measured on strain gauge no. 1, ε_{CFRP}, is below $4 \cdot 10^{-3}$. For a greater bond length equal to 300mm, the maximum strain value recorded on strain gauge no. 1 is approximately $7.05 \cdot 10^{-3}$.

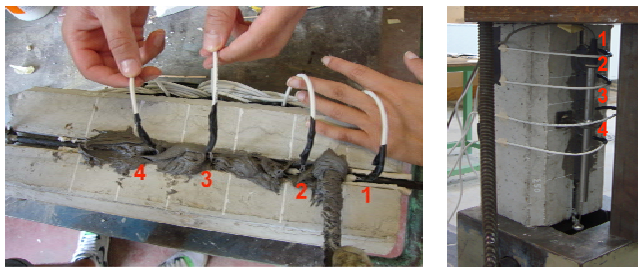

Fig. 2. (a) Setup of direct pull-out test and (b) location of strain gauges.

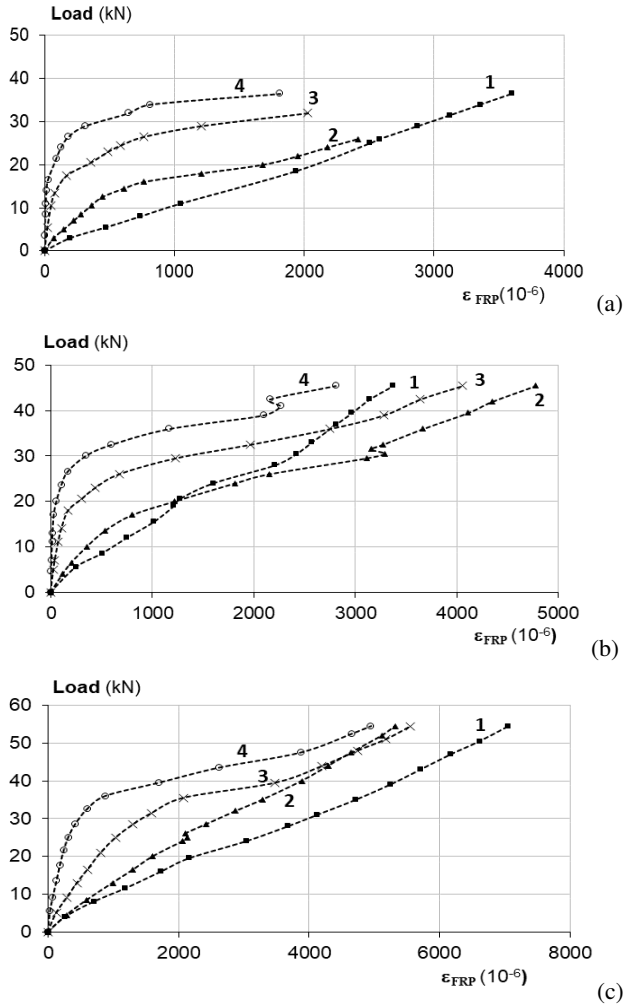

Fig. 3. Exp. load vs strain values by pull-out tests on RC specimens strengthened with the NSM CFRP rod with bond length (a) 200mm; (b) 250mm and (c) 300mm.

The experimental laws shear stress, τ, versus slip, w, were calculated by a numerical procedure considering the measured data of strains; in Figure 4 the experimental law obtained for the specimen with bond length equal to 300mm is compared with the theoretical curve proposed in literature [2,9].

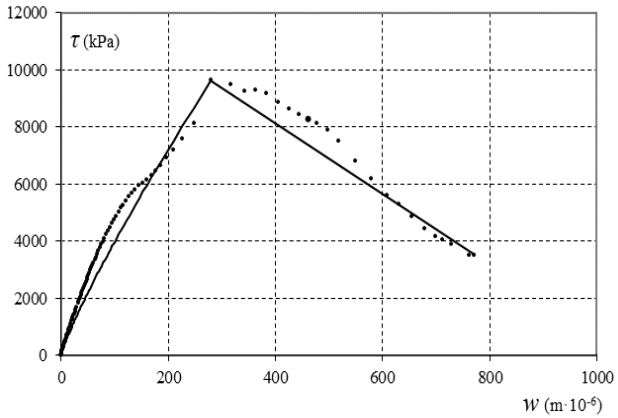

Fig. 4. Theoretical – continuous line – and experimental - dashed line- interface diagrams shear stress, τ, vs slip, w, with bond length l_b=300mm.

The bond adhesion diagram having the greatest fracture energy was selected to evaluate the following value: $G_f \approx 4.64$N/mm. Assuming this fracture energy, the maximum strain of a circular rod can be determined from Eq. (6) obtaining $\varepsilon_{b,\max} = \sqrt{\frac{8 \cdot G_f}{E_b \cdot d_b}} \cong 5.36 \cdot 10^{-3}$ which may be referred to as the value at the onset of delamination.

Experimental results of the pull-out test with GFRP rods lead to lower values of fracture energy with higher maximum slip. In this case, the experimental shear stress versus slip diagrams are substantially linear. It appears that the bond between GFRP rods-resin-concrete is maintained up to the failure of the rod with bond shear stress values about 11.0 N/mm^2; fracture energy values vary between G_f = 1.37÷1.56 N/mm. By comparing the results obtained on pull-out tests, we can conclude that the failure due to the loss of bond seems a relevant mechanism of damage, in particular utilizing the NSM GFRP rod.

3 Static and vibration tests on RC beams

Static tests were planned in laboratory in different phases utilising RC beams with the geometric and mechanical characteristics described below. The dimensions of the beam's sections are 150mm·220mm and measure 1700mm in length (Fig. 5). The steel reinforcement used was 4 bars measuring10mm and stirrups at the interval of 60mm having a diameter of 6mm. Several beams were damaged by bending tests and, successively, strengthened with CFRP circular rods into rectangular grooves measuring 20mm·20mm in section. Other RC beams without damage due to cracking were strengthened with GFRP rods and subjected to bending path and at each step of loading analysed by free vibration tests.

Below, experimental results are discussed for one RC beam strengthened with the CFRP rod without the initial damage degree.

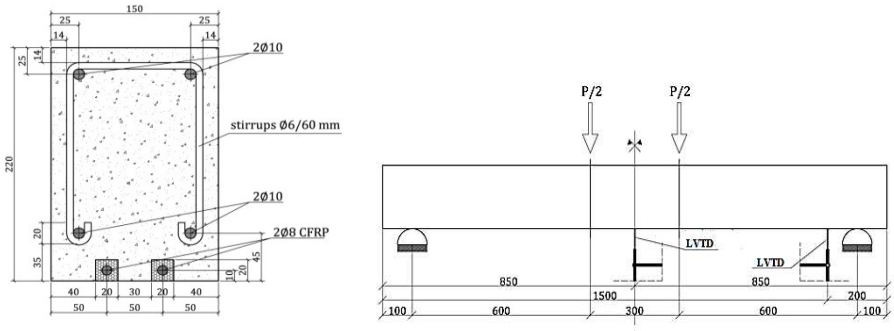

Fig. 5. Setup of the bending static test for the RC beam strengthened with CFRP.

Every cyclic loading corresponds to the so-called damage degree D_i with i=1,…,5-7: Damage D_1-P_1= 7.1kN ; D_2-P_2=14.3kN ; D_3-P_3=31.4kN ; D_4-P_4=39.0kN ; D_5-P_5=87.5kN ; D_6-P_6=105kN ; D_7-failure load P_7=115kN.

The failure of the strengthened RC beam was reached at the load value equal to P=115.0 kN; the failure was due to the crash of the compressive edge of concrete. The strength of the RC beam with NSM CFRP rods compared with an analogous beam without strengthening is more than double.

The experimental measures of strain ε_{CFRP} on CFRP rods at the midspan of the beam confirm that the recorded values reached values equal to $\varepsilon_{CFRP} \approx 4.0\text{x}10^{-3}$ without any damage due to the loss of bond of CFRP rods (Fig. 6).

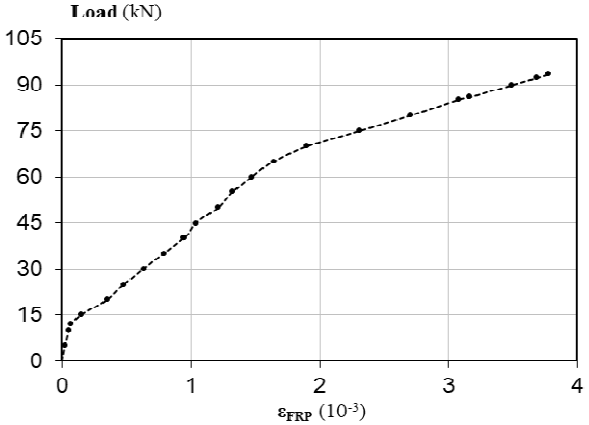

Fig. 6. Exp. diagram load vs strain on the CFRP rod at the mid-length cross section of the strengthened beam.

Finally, experimental free vibration tests were carried out on beams in order to evaluate the influence on the dynamic response of beams of cracking and/or the loss of bond of CFRP rods. The experimental dynamic test was carried out using a specific impact hammer (Fig. 7) using the well-known technique where a mobile accelerometer measures the acceleration of the structural element triggered using a hammer in a fixed point. It was determined that the specimens would be tested dynamically in free-free edge condition. In Figure 7, the setup of vibration tests with the location of measuring instruments is shown. In Figure 8, experimental results are shown with the envelope of FRFs at different damage degrees Di, i=1,…,6 due to bending tests. The transition of the diagram to the left along with the increase in the level of load is evident.

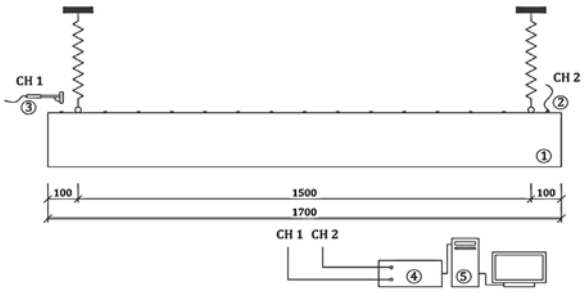

Fig. 7. Setup of dynamic tests: 1. Beam - 2. Accelerometer – 3. Impact hammer – 4. FFT analyzer – 5. PC.

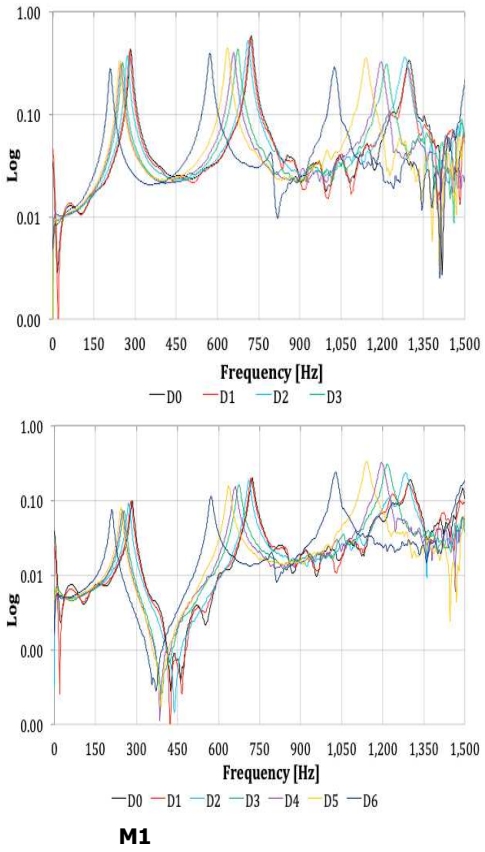

Fig. 8. Envelope of FRFs at different damage degrees Di, i=1,…,6 due to bending tests for CFRP strengthened RC beam recorded with accelerometer in two points M1 and M3.

In the second phase of the investigation, the static and dynamic response of the RC beam damaged by bending loading with and without the NSM GFRP rod strengthening was analysed. The RC beam of 2.20m length and the rectangular section of 120mm·160mm was reinforced with similar steel bars and only one GFRP circular rod, inserted after static tests without strengthening, into the rectangular groove of the 20mm·20mm section.

The RC beam was firstly subjected to the bending test without the GFRP strengthening, according to the setup of a simply supported beam with hinge restraints. The instrumentation used was as follows: one vertical jack and one load cell to evaluate the vertical load value during the bending test; three LVDTs to measure deflections at midspan and close to restraints; LVDTs to record strains at the midspan of beams at the top and bottom on the midspan section (Fig. 9).

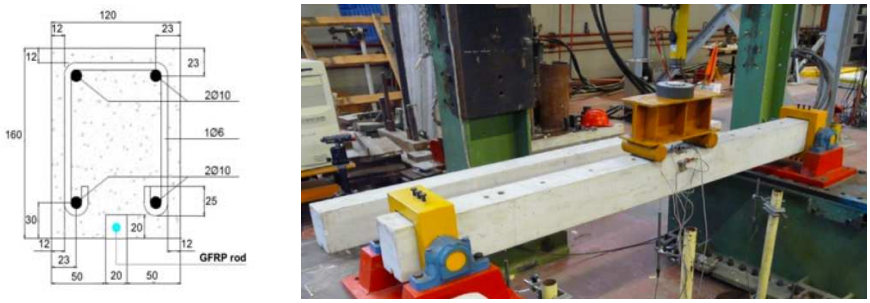

Fig. 9. Setup of static bending tests for simply supported RC beam with and without the GFRP rod.

The RC beam was subjected to three loading and unloading cycles: D_1-P_1=4kN, D_2-P_2=8kN, D_3-P_3=18kN. The choice of these load cycles permitted to damage the beam with cracks on concrete reaching the maximum experimental value of steel strain equal to $\varepsilon_s \cong 3.35 \cdot 10^{-3}$ for damage degree D3, higher than the yield strain value of steel. After D_3 damage degree, the RC beam was strengthened with a GFRP circular rod inserted in the groove by adhesive epoxy resin and subjected to a similar loading path for the load step D_1, D_2 and D_3. Successively, the beam was subjected to increasing load until failure.

The collapse, reached at a load value equal to P=33 kN, occurred with the crushing of the compressed concrete and successively the expulsion of the concrete cover at the intrados with the detachment of the GFRP rod. The evolution of the strain on the GFRP rod was monitored through a strain gauge glued on the rod's surface at the midspan section of beam. The experimental measures of strain ε_{GFRP} on GFRP rods highlight that the recorded values reached a maximum equal to $\varepsilon_{GFRP} \approx 6.0 \text{x} 10^{-3}$ before the collapse (Fig. 10).

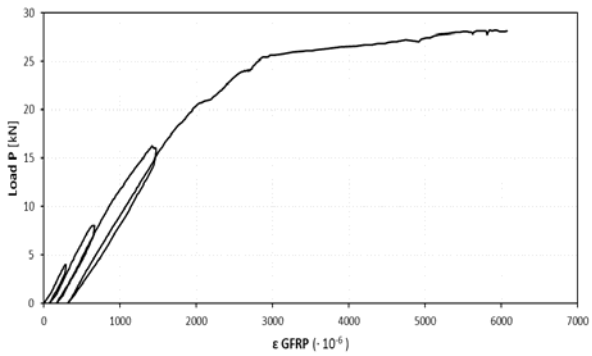

Fig. 10. Exp. diagram load vs strain on GFRP rod at mid length cross section of the strengthened beam.

Finally, experimental free vibration tests were carried out on the beam in order to evaluate the influence on the dynamic response of beams of cracking and/or the loss of bond of GFRP rods. The dynamic responses were obtained using, once again, the same methodology described above with the impact by hammer and an accelerometer at 9 nine

measurement points connected to an acquisition system working in a range of frequencies between 0 and 1500 Hz. The signals were recorded and elaborated in the frequency domain through the FFT technique and FRFs obtained using Pulse software. The un-strengthened and GFRP strengthened beam was dynamically tested in free-free ends condition. The FRF envelope recorded during free vibration tests for each step of damage degree is shown in Figure 11 for both configurations.

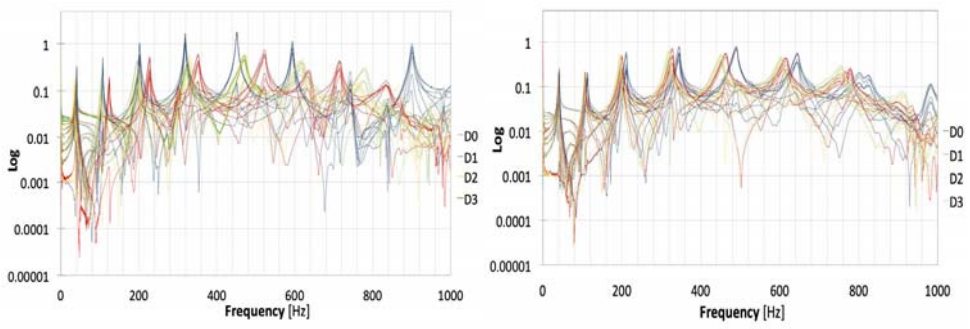

Fig. 11. Envelope of FRFs for (a) un-strengthened and (b) GFRP strengthened beam at different damage degrees D_i=0, 1…, 3.

As seen from the envelope diagrams of FRFs, there was a progressive lowering of frequency values from the undamaged degree D_0 up to the damage degree D_3. The comparison of frequency variations for the response of GFRP strengthened beam shows that the difference between the peak frequency for different damage degrees is rather small. In fact, the application of the NSM GFRP strengthening contributes to reducing the width of the cracks undergoing even heavy loads.

4 Conclusions

A large investigation on specimens with NSM C-GFRP rods and subjected to pull-out tests, bending tests and vibration tests allowed to analyze the structural response of strengthened RC elements. Experimental static and vibration results are discussed and comments on the strengthening bond of NSM C-GFRP rods were developed. Main conclusions of investigations can be summarized as follows:

- the failure due to the loss of bond seems a relevant mechanism of damage, in particular utilizing the NSM GFRP rod;
- combined static and dynamic experimental measures confirm that beams strengthened with the NSM C-GFRP rod under service loads present an adequate response without relevant capacity decrease;
- frequency variations are relatively low in strengthened RC beams with the NSM C-GFRP rod while the variations are high when the RC beams are strengthened only with steel reinforcement, due to the FRP capacity to limit the cracking damage state under bending conditions.

This experimental research was supported by research funds provided by Università Politecnica delle Marche. The authors would like to express their gratitude to all the technicians and students who collaborated to develop the experimental research.

References

1. L. De Lorenzis, A. Nanni, ACI Struct. J. **99,** 2, 123-132 (2001).
2. L. De Lorenzis, J. G. Teng, Comp. P. B: Eng. **38**, 119-143 (2007).
3. R. Kotynia, In Proc. 3rd Int. Conf.: Composite in Construction 2005, Lyon, July 2005.
4. R. El-Hacha, S. Rizkalla, ACI Struct. J. **101,** 5, 717-726 (2004).
5. L. De Lorenzis, A. Nanni, ACI Struct. J. **99**, 123-133 (2002).
6. I. A. Sharaky, L. Torres, M. Baena, C. Miàs, Comp. Struct. **99**, 350-365, 2013.
7. J. M. Sena Cruz, J. A. O. Barros, R. Gettu, A. F. M. Azevedo, ASCE J. of Comp. for Constr. **10**, 295-303 (2006).
8. R. Capozucca, Comp. Struct. **102**, 110-123 (2013).
9. L. De Lorenzis, A. Rizzo, A. La Tegola, Comp. P. B: Eng. **33**, 589-603 (2002).
10. F. Focacci, A. Nanni, C.E. Bakis, ASCE J. of ComP. for Constr. **4**, 24-31 (2000).
11. R. Capozucca, Comp. Struct. **91**, 237-248 (2009).
12. R. Capozucca, Comp. P. B. **46**, 69-80 (2013).
13. R. Capozucca, Comp. Struct. **102**, 110-123 (2013).
14. R. Capozucca, Comp. Struct. **117**, 143-155 (2014).
15. B. Baghiee, M. R. Esfahani, K. Moslem, Eng. Struct. **31**, 875-893 (2009).
16. O. S. Salawu, Eng. Struct. **19**, 718-723 (1997).
17. ASTM D 3039/D 3039 M - 08. American Standard of Testing and Materials (2008).
18. G. B. Warburton. *The dynamical behaviour of structures*. Pergamon Press, 1964, Oxford.